

## Experimental tests of paleoclassical transport

This article has been downloaded from IOPscience. Please scroll down to see the full text article.

2007 Nucl. Fusion 47 1449

(<http://iopscience.iop.org/0029-5515/47/11/006>)

View [the table of contents for this issue](#), or go to the [journal homepage](#) for more

Download details:

IP Address: 128.104.166.214

The article was downloaded on 13/10/2010 at 22:10

Please note that [terms and conditions apply](#).

# Experimental tests of paleoclassical transport

J.D. Callen<sup>1</sup>, J.K. Anderson<sup>1</sup>, T.C. Arlen<sup>2,3</sup>, G. Bateman<sup>4</sup>,  
 R.V. Budny<sup>5</sup>, T. Fujita<sup>6</sup>, C.M. Greenfield<sup>3</sup>, M. Greenwald<sup>7</sup>,  
 R.J. Groebner<sup>3</sup>, D.N. Hill<sup>3</sup>, G.M.D. Hogewij<sup>8</sup>, S.M. Kaye<sup>5</sup>,  
 A.H. Kritiz<sup>4</sup>, E.A. Lazarus<sup>3,9</sup>, A.C. Leonard<sup>3</sup>, M.A. Mahdavi<sup>3</sup>,  
 H.S. McLean<sup>10</sup>, T.H. Osborne<sup>3</sup>, A.Y. Pankin<sup>4</sup>, C.C. Petty<sup>3</sup>,  
 J.S. Sarff<sup>1</sup>, H.E. St John<sup>3</sup>, W.M. Stacey<sup>11</sup>, D. Stutman<sup>12</sup>,  
 E.J. Synakowski<sup>10</sup> and K. Tritz<sup>12</sup>

<sup>1</sup> University of Wisconsin, Madison, WI 53706-1609, USA

<sup>2</sup> California Polytechnic State University, San Luis Obispo, CA 93407, USA

<sup>3</sup> General Atomics, San Diego, CA 92186-5608, USA

<sup>4</sup> Lehigh University, Bethlehem, PA 18015-3182, USA

<sup>5</sup> Princeton Plasma Physics Laboratory, Princeton, NJ 08543-0451, USA

<sup>6</sup> Naka Site, JAEA, 801-1 Mukouyama, Naka, Ibaraki-ken 311-0193, Japan

<sup>7</sup> Massachusetts Institute of Technology, Cambridge, MA 02139, USA

<sup>8</sup> FOM Institute for Plasma Physics Rijnhuizen, 3430 BE Nieuwegein, The Netherlands

<sup>9</sup> Oak Ridge National Laboratory, Oak Ridge, TN 37831, USA

<sup>10</sup> Lawrence Livermore National Laboratory, Livermore, CA 94551-0808, USA

<sup>11</sup> Georgia Tech, Atlanta, GA 30332, USA

<sup>12</sup> Johns Hopkins University, Baltimore, MD 21218, USA

E-mail: [callen@engr.wisc.edu](mailto:callen@engr.wisc.edu)

Received 31 January 2007, accepted for publication 20 August 2007

Published 10 October 2007

Online at [stacks.iop.org/NF/47/1449](http://stacks.iop.org/NF/47/1449)

## Abstract

Predictions of the recently developed paleoclassical transport model are compared with data from many toroidal plasma experiments: electron heat diffusivity in DIII-D, C-Mod and NSTX ohmic and near-ohmic plasmas; transport modelling of DIII-D ohmic-level discharges and of the RTP ECH ‘stair-step’ experiments with electron internal transport barriers (eITBs) at low order rational surfaces; investigation of a strong eITB in JT-60U; H-mode  $T_e$  edge pedestal properties in DIII-D; and electron heat diffusivities in non-tokamak experiments (NSTX/ST, MST/RFP, SSPX/spheromak). The radial electron heat transport predicted by the paleoclassical model is found to be in reasonable agreement with a wide variety of ohmic-level experimental results and to set the lower limit (within a factor  $\lesssim 2$  in tokamaks) on the radial electron heat transport in most resistive, current-carrying toroidal plasmas—for  $T_e \lesssim T_e^{\text{crit}} \simeq B^{2/3} \bar{a}^{1/2}$  keV where it is expected to be dominant over fluctuation-induced anomalous transport that scales with a gyro-Bohm diffusion coefficient.

**PACS numbers:** 52.55.Fa, 52.55.Dy, 52.25.Fi, 52.55.Ip

## 1. Introduction

A new model for an irreducible minimum level of radial electron heat transport, the paleoclassical model, was introduced at the 2004 IAEA Vilamoura meeting [1]; its basic features [2] and details [3] are now published. The key hypothesis of the model is that in resistive, current-carrying toroidal plasmas, electron guiding centres diffuse radially with thin annuli of poloidal magnetic flux on the magnetic (‘skin’)

diffusion time scale. This key hypothesis was originally motivated phenomenologically [3]; a derivation of it has been published recently [4].

This paper carries the initially encouraging comparisons with experimental data [1] to a higher level via a number of more detailed comparisons of paleoclassical electron heat transport with data from a variety of toroidal plasma experiments—about half the 19 tests in 5 categories proposed in [1]. It also seeks to determine the situations (mainly

ohmic-level plasmas and in the cooler plasma edge) where paleoclassical radial electron heat transport is dominant.

In devising experimental tests, it is important to recognize that the paleoclassical model provides a *minimum* level of radial electron heat transport—analogueous to how the neoclassical model provides the minimum level of ion heat transport. Since the paleoclassical diffusivity scales with  $T_e^{-3/2}$  in many collisionality regimes, it typically decreases as a plasma is heated; hence it does not often provide the transport mechanism that limits plasma confinement. Thus, like neoclassical ion heat transport, it cannot usually be probed by analysing responses to additional heating or via global scaling law studies. Rather, the most effective way to test it against experimental data will be to compare the inferred radial electron heat diffusivity against the paleoclassical model predictions in situations where fluctuation-induced anomalous transport is likely to be minimal—most typically in low  $T_e$  ohmic-level and edge plasmas.

Most comparisons will be made with well-characterized, previously published experimental data. In general, ‘typical best case’ comparisons are shown in the figures; the text comments on other comparisons and on some cases where the paleoclassical model does not represent the experimental data well. The main comparisons are between the radial electron heat diffusivities predicted by the paleoclassical model and those inferred from ‘power balance’ analyses; since typical error bars in both the theory [1–3] and experimental data analysis are of order a factor of two, agreement within this margin will be considered satisfactory. Some dynamic modelling tests are also presented.

## 2. Brief summary of paleoclassical model

The paleoclassical radial electron heat transport to be added to the right of an electron energy balance equation is [1, 3]

$$-\langle \nabla \cdot \mathbf{Q}_e^{\text{pc}} \rangle = \frac{M+1}{V'} \frac{\partial^2}{\partial \rho^2} \left( V' \frac{\eta_{\parallel}^{\text{nc}}}{\mu_0 \bar{a}^2} \frac{3}{2} n_e T_e \right), \quad (1)$$

in which  $\rho$  is a dimensionless radial coordinate based on the square root of the toroidal magnetic flux and  $V' \equiv dV/d\rho$  in which  $V(\rho)$  is the volume of the  $\rho$  flux surface. The implied approximate radial electron heat diffusivity  $\chi_e^{\text{pc}}$  and magnetic field diffusivity  $D_\eta$  (both in  $\text{m}^2 \text{s}^{-1}$ ) are [1, 3]

$$\chi_e^{\text{pc}} \equiv \frac{3}{2} (M+1) D_\eta, \quad D_\eta \equiv \frac{\eta_{\parallel}^{\text{nc}}}{\mu_0} \sim \frac{\eta_0}{\mu_0} \equiv \frac{1400 Z_{\text{eff}}}{T_e (\text{eV})^{3/2}}. \quad (2)$$

Here,  $\eta_{\parallel}^{\text{nc}}$  is the neoclassical parallel resistivity, the unity in  $M+1$  represents the axisymmetric contribution [3], and the helical multiplier  $M$  [3] is

$$M = \frac{\min\{\ell_{\text{max}}, \lambda_e, \ell_{n^\circ}\}}{\pi \bar{R} q} \simeq \frac{1}{\pi \bar{R} q} \frac{1}{1/\lambda_e + 1/\ell_{\text{max}}}. \quad (3)$$

The formula after the  $\simeq$  indicates an appropriate smoothing formula for  $M$ . It is appropriate in the usual case where  $\ell_{n^\circ} \equiv \pi \bar{R} q^\circ n^\circ$  (in which  $n^\circ = 1, 2$  near a low order rational surface  $q^\circ \equiv m^\circ/n^\circ$ ) is not relevant—because of its radial extent being very narrow with strong magnetic shear [1, 3] and/or because the plasma is not steady for at least a global magnetic diffusion time scale, as discussed at the end of the

first paragraph in section 5. In (1) the average minor radius  $\bar{a}$  is defined by [1, 3]

$$\frac{1}{\bar{a}^2} \equiv \frac{\langle |\nabla \rho|^2 / R^2 \rangle}{\langle R^{-2} \rangle} \simeq \frac{1}{a^2} \frac{1 + \kappa^2}{2 \kappa^2}. \quad (4)$$

The formula at the end gives an approximate formula for elliptical cross-section plasmas with  $\kappa \equiv b/a \geq 1$ . Further,  $\lambda_e \equiv v_{T_e}/\nu_e \simeq 1.2 \times 10^{16} T_e (\text{eV})^2 / n_e (\text{m}^{-3}) Z_{\text{eff}}$  m is the electron collision length and  $\ell_{\text{max}}$  is the length over which magnetic field lines diffuse radially [1, 3]:

$$\ell_{\text{max}} = \pi \bar{R} q n_{\text{max}}, \quad n_{\text{max}} = (\pi \bar{\delta}_e |q'|)^{-1/2}; \quad (5)$$

$$\max\{n_{\text{max}}\} = (\pi^2 \bar{\delta}_e^2 |q''|)^{-1/3}, \quad \text{when } |q'| \simeq 0. \quad (6)$$

Here,  $q' \equiv dq(\rho)/d\rho$  and  $q'' \equiv d^2q/d\rho^2$  are both dimensionless, and  $\bar{\delta}_e \equiv c/\omega_p \bar{a}$  is the normalized (dimensionless) electromagnetic skin depth. Limiting regimes of the paleoclassical electron heat diffusivity are

I. collisionless ( $\lambda_e > \ell_{\text{max}}$ ):  $\chi_{\text{el}}^{\text{pc}} = \frac{3}{2} \frac{\eta_{\parallel}^{\text{nc}}}{\mu_0} n_{\text{max}}, \quad (7)$

II. collisional ( $\ell_{\text{max}} > \lambda_e > \pi \bar{R} q$ ):  $\chi_{\text{el}}^{\text{pc}} = \frac{3}{2} \frac{v_{T_e}}{\pi \bar{R} q} \frac{c^2}{\omega_p^2} \frac{\eta_{\parallel}^{\text{nc}}}{\eta_0}, \quad (8)$

III. edge ( $\pi \bar{R} q > \lambda_e > \pi R$ ):  $\chi_{\text{el}}^{\text{pc}} \simeq \frac{10^3 Z_{\text{eff}}}{T_e (\text{eV})^{3/2}}. \quad (9)$

Because  $\chi_e^{\text{pc}}$  scales with the magnetic field diffusivity  $D_\eta = \eta_{\parallel}^{\text{nc}}/\mu_0$ , it scales mainly as  $\bar{a}^{1/2} T_e^{-3/2}$  in the collisionless regime (I) and thus usually decreases as  $T_e$  increases. In contrast, drift-wave-type instabilities (ITG, DTEM, ETG) induce micro-turbulence and anomalous heat transport, which scale with the gyro-Bohm coefficient [1]  $\chi_e^{\text{gB}} \simeq f_{\#} 3.2 T_e (\text{keV})^{3/2} A_1^{1/2} / \bar{a} B^2 \text{m}^2 \text{s}^{-1}$ , that increases as  $T_e$  increases. While the dimensionless coefficient  $f_{\#}$  is in general a threshold-type function and not well quantified, ITG simulations often find  $\chi_e/\chi_i \lesssim 1/3$  and experimental results (see figure 10 of [5] from TCV) indicate  $f_{\#} \lesssim 1/3$ , for all  $R/L_{T_e} \equiv R|d \ln T_e / dr|$ . Using  $f_{\#} \simeq 1/3$ , we can anticipate [1] that, roughly speaking, below some  $T_e$ ,

$$T_e \lesssim T_e^{\text{crit}} \simeq B(T)^{2/3} \bar{a} (\text{m})^{1/2} (3 f_{\#})^{-1/3} \quad (10)$$

$$\simeq B^{2/3} \bar{a}^{1/2} \text{keV}, \text{ paleoclassical dominant.} \quad (11)$$

Fortunately,  $T_e^{\text{crit}}$  depends on only the one-third power of the unknown coefficient  $f_{\#}$ . Because paleoclassical transport is most likely to be dominant at low  $T_e$ , we explore transport comparisons mainly in lower  $T_e$  ohmic-level and edge plasmas.

While  $\chi_e^{\text{pc}}$  scales with the perpendicular electrical resistivity  $\eta_0$ , which decreases as  $T_e^{-3/2}$ , it is important to realize that in some regimes  $\chi_e^{\text{pc}}$  can increase with  $T_e$  and provide the limiting electron heat transport. For example, in the ‘collisional’ regime (II: Alcator scaling [1, 2])  $\chi_{\text{el}}^{\text{pc}} \propto T_e^{1/2}$ . Also, trapped particle effects increase the parallel neoclassical to perpendicular resistivity factor  $\eta_{\parallel}^{\text{nc}}/\eta_0$  as the neoclassical collisionality parameter  $\nu_{*e} \equiv \nu_e / [\epsilon^{3/2} (v_{T_e}/R_0 q)]$  decreases with increasing  $T_e$  [1, 3]; hence, they can cause both  $\eta_{\parallel}^{\text{nc}}/\eta_0$  and  $\chi_e^{\text{pc}}$  to increase (slightly) with increasing  $T_e$ . Thus, paleoclassical transport can sometimes become the limiting transport process—most likely in high density ohmic-level plasma regimes such as those accessed in the Alcator experiments.

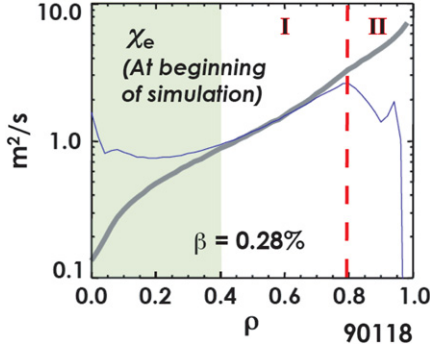


**Figure 1.** DIII-D electron heat diffusivity in ohmic-level beta-scan [6] discharge: analysis (thick grey line), paleo (thin blue line), sawtooth region (shaded).

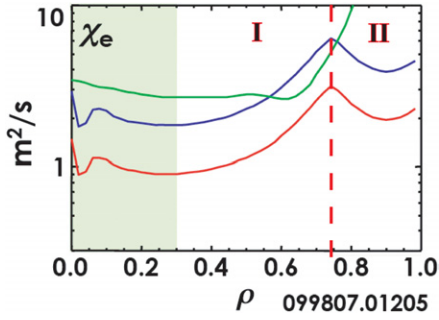


**Figure 2.** DIII-D electron heat diffusivity in LOC regime [12, 13]: analysis (green, dimmest), paleo (red, dark),  $2 \times$  paleo (blue).

### 3. DIII-D confinement region electron heat diffusivity comparisons

Comparisons of paleoclassical predictions with  $\chi_e^{\text{pb}} \equiv \langle Q_e \cdot \nabla V \rangle / \langle -n_e \nabla T_e \cdot \nabla V \rangle$  experimental ‘power balance’ analysis data are most appropriate in the confinement region of tokamak plasmas,  $0.4 \lesssim \rho \lesssim 0.9$ , because sawteeth often occur for  $\rho \lesssim 0.4$  and transport data typically have large uncertainties for  $\rho \gtrsim 0.9$ . In the confinement region, tokamak plasmas are usually in the ‘collisionless’ (I) paleoclassical regime [1] where  $\ell_{\text{max}}$  dominates in (3) and  $M = n_{\text{max}} \sim 10$ . Comparisons of  $\chi_e^{\text{pc}}$  with experimental  $\chi_e^{\text{pb}}$  data from 6 of the base ohmic-level ( $T_e(0.4) \lesssim T_e^{\text{crit}} \sim 1\text{--}1.35$  keV) discharges in DIII-D beta [6] and collisionality [7] scans show reasonable agreement [8, 9]—similar profiles and plasma parameter scaling, and usually within a factor of about 2 in magnitude (but low by a factor  $\sim 3$  for low collisionality where  $T_e(0.4) \gtrsim T_e^{\text{crit}}$ ), except near the edge. A ‘typical best case’ comparison is shown in figure 1. Here,  $\chi_e^{\text{pc}}$  decreases towards the edge ( $\rho \gtrsim 0.8$  in figure 1) because the collision length  $\lambda_e$  becomes less than  $\ell_{\text{max}}$  and one transitions to the ‘collisional’ (II: Alcator scaling) paleoclassical regime where  $M = \lambda_e / \pi \bar{R} q$  and  $\chi_{\text{eII}}^{\text{pc}} \propto T_e^{1/2} / n_e q$ . The increase of  $\chi_e^{\text{pb}}$  with  $\rho$  there could be caused by anomalous plasma transport induced by resistive ballooning modes (RBMs) [10, 11] in this  $T_e \lesssim 300$  eV region of these ohmic L-mode plasmas.

Figure 2 shows a similar comparison [9] for a DIII-D plasma in the linear ohmic confinement (LOC) regime

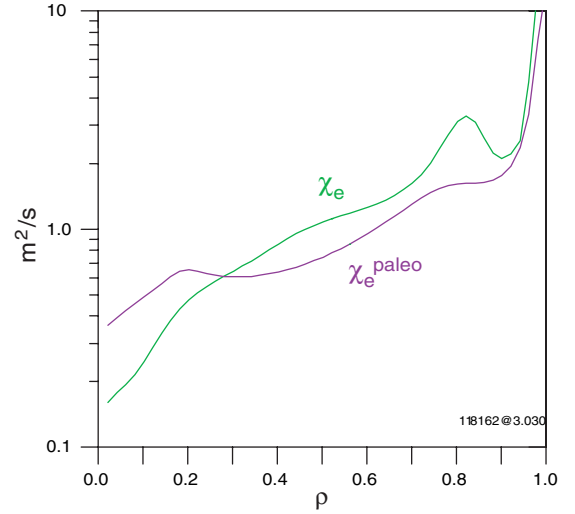


**Figure 3.** Profile of  $\chi_e$  just before a sawtooth crash in DIII-D bean-shaped plasma [15].

[12, 13] where  $\tau_E \sim n_e$  and one would expect [1–3] to be in the collisional (II: Alcator scaling) regime; while the agreement is reasonable over the critical region (for overall energy confinement) of  $0.5 \lesssim \rho \lesssim 0.8$ , this plasma is only marginally in the paleoclassical collisional regime there. A comparison [9] in a higher density saturated ohmic confinement (SOC) discharge, in which ITG turbulence was inferred to be present [12, 13], found  $\chi_e^{\text{pc}}$  to be about the right magnitude, but with the wrong (collisional) profile over this same radial region.

Dynamic ONETWO modelling of all these DIII-D discharges (from  $\rho = 0.9$  inwards) using the paleoclassical transport model yields  $T_e$  profiles in reasonable agreement with the experimental ones (to within  $\lesssim 20\%$ ) where  $T_e \lesssim T_e^{\text{crit}}$ . However, ‘thermal run away’ occurs in dynamic simulations without a sawtooth model in the central, sawtoothing region  $\rho \lesssim 0.4$  because the collisionless  $\chi_{\text{eI}}^{\text{pc}} \propto T_e^{-3/2}$ , which is applicable there, decreases with increasing  $T_e$ .

Comparisons with DIII-D ‘hybrid’ discharges [14] at  $\rho \sim 0.5$  where one has  $(T_e / T_e^{\text{crit}})^3 \gtrsim (2.5 \text{ keV} / 1.3 \text{ keV})^3 \simeq 7 \gg 1$  show [8, 9] that  $\chi_e^{\text{pc}}$  is a factor of 5–7 too small and has a different profile from  $\chi_e^{\text{pb}}$  for these discharges, which have micro-turbulence fluctuations (presumably due to ITG modes) and 3/2 NTMs in them. Thus, we conclude that for DIII-D ohmic-level plasmas the paleoclassical model predicts the  $\chi_e$  magnitude and profile ( $\lesssim$  factor of 2) and  $T_e$  profile within the confinement region—as long as  $T_e \lesssim T_e^{\text{crit}}$  there.

There are, however, situations in DIII-D where  $\chi_e^{\text{pc}}$  sets the minimum level of transport even when  $T_e^3 \gg (T_e^{\text{crit}})^3$ . Figure 3 shows such a case; it was obtained with a bean-shaped cross-section DIII-D plasma developed for sawtooth studies [15, 16]. At the time shown (just before a sawtooth crash) it has  $[T_e(0) / T_e^{\text{crit}}]^3 \simeq (2.5 \text{ keV} / 1.3 \text{ keV})^3 \simeq 7 \gg 1$ . Also, figure 4 shows that the core-averaged  $\chi_e$  decays down to the paleoclassical level just before the next sawtooth crash. In a corresponding oval cross-section DIII-D plasma the  $\langle \chi_e^{\text{pb}} \rangle$  values were much higher earlier in time, but again decreased to  $\langle \chi_e^{\text{pc}} \rangle$  just before the next sawtooth crash (see figure 24 of [16]).

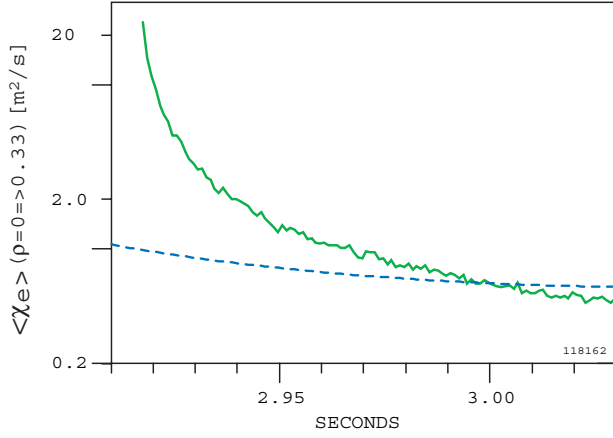


**Figure 4.** Core-average  $\chi_e$  decays to the paleoclassical prediction between sawtooth crashes (at 2.9 and 3.04 s): analysis (green, solid), paleo (blue dashed) [15, 16].

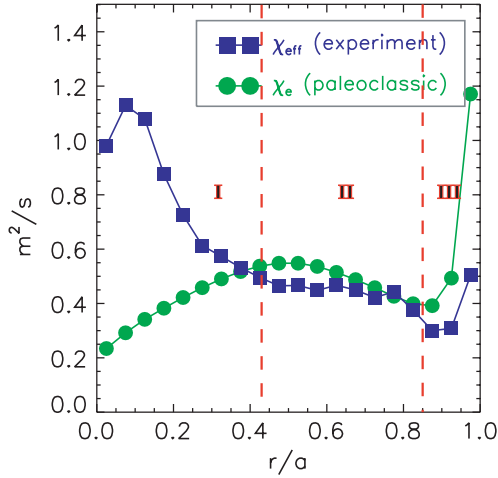


**Figure 5.** Electron heat diffusivity profile for C-Mod H-mode shot 960116027 [17].

#### 4. C-Mod electron heat diffusivity, critical $T_e$ gradient and power flow

Alcator C-Mod operates at higher magnetic field and thus has a higher  $T_e^{\text{crit}}$ —about 1.6 keV for  $B \simeq 5.3$  T and  $\bar{a} \simeq 0.27$  m. Figure 5 shows a comparison of  $\chi_e^{\text{pc}}$  with the experimental  $\chi_{\text{eff}}$ , which includes both electron and ion heat diffusivities, for a well-diagnosed H-mode discharge [17]. For this discharge, sawteeth influence  $\rho \gtrsim \rho_{\text{inv}} \simeq 0.35$ ; also,  $T_e \lesssim T_e^{\text{crit}} \simeq 1.6$  keV for  $\rho > 0.45$ . Figure 5 shows  $\chi_e^{\text{pc}}$  agrees well with C-Mod H-mode data in all three regimes in (7)–(9): collisionless (I) for  $\rho < 0.43$ , collisional (II) for  $0.43 < \rho < 0.85$  and edge (III) for  $\rho > 0.85$ . Similar agreement is also obtained for an L-mode discharge [17].

The original paleoclassical papers [1] noted that the paleoclassical electron heat transport operator in (1) naturally includes heat pinch or minimum temperature gradient effects. Specific forms for them were given [1, 3] under the assumption that  $M + 1$  varies little with  $\rho$ . However,  $M$  varies significantly for the C-Mod data in figure 5—from  $\sim 15$  for  $\rho < 0.43$  down to  $< 1$  for  $\rho > 0.85$ . Thus, attempts to compare the critical  $T_e$  gradient scale length in equation (58) of [1] with the data in

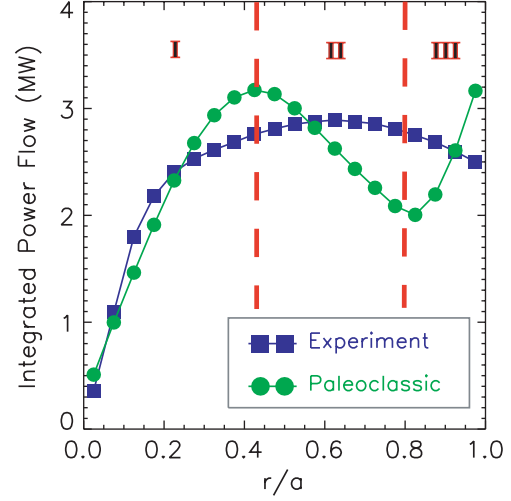


**Figure 6.** Radial electron power flow versus radius for C-Mod H-mode shot 960116027 [17].

figure 5 failed, except for  $\rho > 0.85$  where it should be valid (because  $M + 1 \simeq 1$  there) and did represent the data. As a check on the form of the paleoclassical transport operator, figure 6 shows that the volume integral of the form in (1) agrees reasonably well with the experimental electron power flow for the H-mode discharge [17] in figure 5.

#### 5. Electron internal transport barriers (eITBs) in RTP and JT-60U

Near a low order rational surface (e.g.  $q^\circ \equiv m^\circ/n^\circ = 2/1$ ),  $l_{n^\circ} \equiv \pi \bar{R} q^\circ n^\circ$  dominates in (3) and  $M \simeq n^\circ$ , which yields [1, 3] electron ‘internal transport barriers’ where  $\chi_e^{\text{pc}}$  is smaller by  $(n^\circ + 1)/n_{\text{max}} \sim 0.2\text{--}0.5$  over widths determined by magnetic shear [1–3], as shown in figure 7. Physically, in the collisionless (I) paleoclassical regime where  $M \simeq \min\{\ell_{\text{max}}, \ell_{n^\circ}\}/\pi \bar{R} q = \min\{n_{\text{max}}, n^\circ\}$ , these eITBs occur around low order rational surfaces because the helically-resonant transport there is proportional to the short length  $\ell_{n^\circ} \equiv \pi \bar{R} q^\circ n^\circ$  of the low order rational field line which leads to  $M \sim n^\circ$ . The region of reduced transport extends radially [3] to within  $\delta_e \equiv c/\omega_p \sim 1$  mm of the nearest  $n_{\text{max}}$  surface where it begins to be influenced by helically-resonant paleoclassical transport around the  $n_{\text{max}}$  surface where the much longer  $\ell_{\text{max}}$  is relevant and  $M$  increases abruptly up to  $n_{\text{max}} \sim 10$ —as indicated in figure 7. These features produce transport barriers like those inferred [18, 19] from the RTP ‘stair-step’ experiments in which the central  $T_e$  decreased abruptly as radially highly localized ECH was moved radially outwards (in steps  $\lesssim 0.01 a$ , in successive shots) past low order rational surfaces. Modelling [20] of such RTP discharges with twice  $\chi_e^{\text{pc}}$  is shown in figure 8. (With  $1 \times \chi_e^{\text{pc}}$  only slightly higher  $T_e(0)$  values and modified  $q$  profiles are obtained.) For most of these cases  $T_e \lesssim T_e^{\text{crit}} \simeq 0.7$  keV over most of the plasma and the collisionless  $\chi_{\text{el}}^{\text{pc}}$  is applicable for  $\rho \lesssim 0.8$ . The paleoclassical model results shown in figure 8 approximate the ‘stair-step’ details of the central temperature  $T_e(0)$  versus deposition radius  $\rho_{\text{dep}}$  reasonably well. (However, the paleoclassical model does not reproduce the slightly hollow  $T_e$  profiles that are observed experimentally

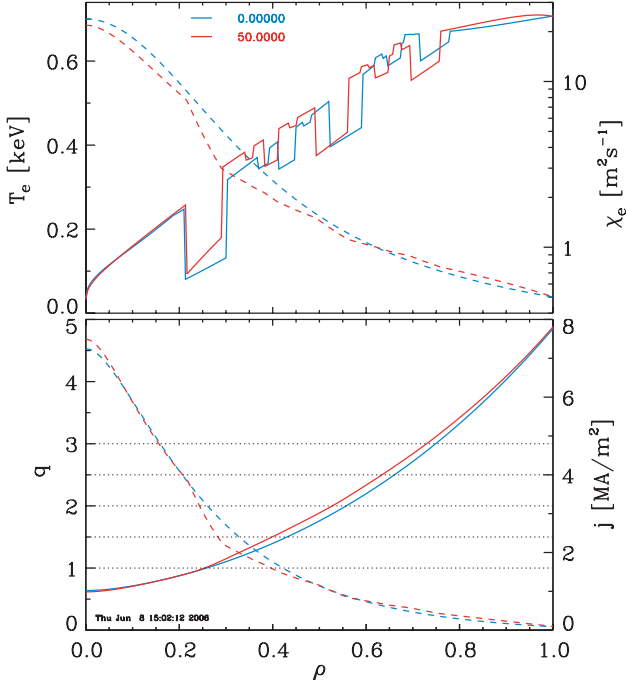


**Figure 7.** Profiles for RTP ohmic discharge: initially (blue, darker experimental  $T_e$ ), paleoclassical modelling at 50 ms (red, lighter). Largest eITBs are at  $q = 1/1, 2/1, 3/1$  [20].

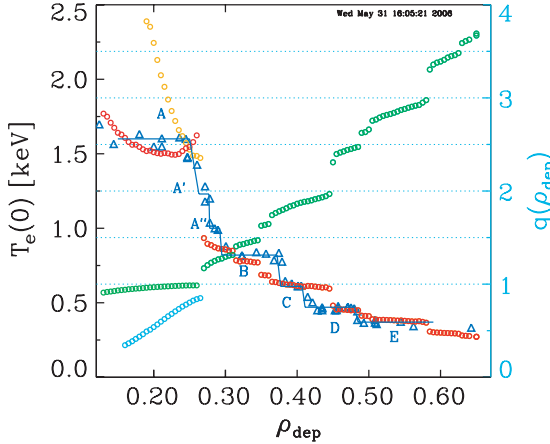


**Figure 8.**  $T_e$  on-axis as ECH deposition is moved radially outwards: RTP experiment (blue triangles), paleoclassical modelling (dark red circles with sawtooth model, light orange circles, without) [20].

for far off-axis ECH which modify the barrier locations a bit [20].) As in the DIII-D dynamic modelling, ‘thermal runaway’ occurs for  $\rho \lesssim 0.25$  (light orange circles in figure 8)—unless a sawtooth  $T_e$  relaxation model is used there (light red circles). The presence of eITBs at low order rational surfaces requires plasmas to come into steady state [18, 19]—apparently on the slow global magnetic diffusion time scale. Paleoclassical modelling [20] of the evolution of two RTP plasmas with very closely spaced ECH deposition radii is shown in figure 9. The corresponding  $T_e$ ,  $q$  and  $\chi_e^{\text{pc}}$  profiles are shown in figure 10. The position sensitivity, temporal behaviour and sharp transport bifurcations are well represented by the modelling of these cases in which the global magnetic field diffusion time is  $\tau_\eta \equiv a^2/6D_\eta(\rho=0) \sim 20$  ms.

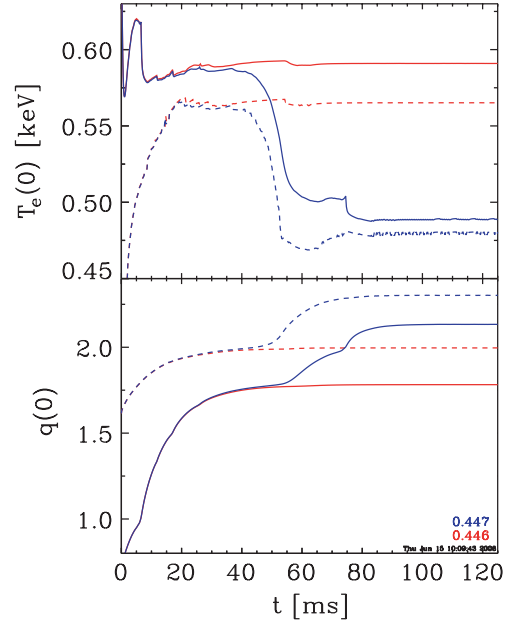


**Figure 9.** Evolution of central  $T_e$ ,  $q$  for ECH  $\rho_{\text{dep}} = 0.446$  (red, light), 0.447 (blue, dark): RTP experiment (—) and paleoclassical modelling (---) [20].

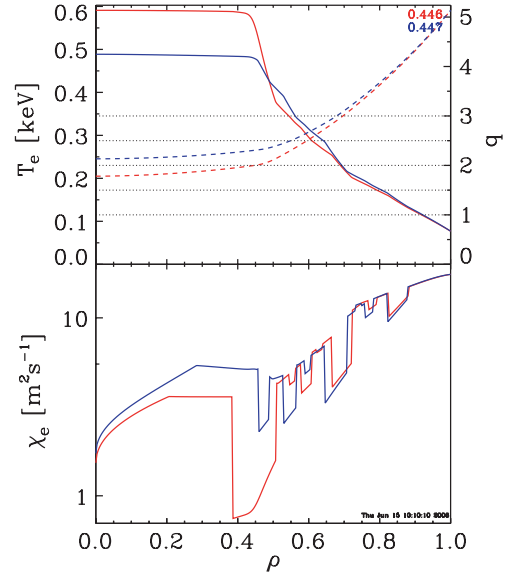


**Figure 10.** Corresponding paleoclassical modelling profiles of  $T_e$ ,  $q$  and  $\chi_e$  for ECH  $\rho_{\text{dep}} = 0.446$  (red, light), 0.447 (blue, dark) in RTP [20].

Similarly, the original paleoclassical papers [1–3] proposed that eITBs produced in DIII-D [21] and JT-60U [22, 23] were induced by an off-axis minimum in  $q$  occurring at a low order rational surface which could cause a small  $\chi_e^{\text{pc}} \sim n^\circ D_\eta$  there. However, in DIII-D at the  $q = 2/1$  surface  $(T_e/T_e^{\text{crit}})^3 \sim (2 \text{ keV}/1.3 \text{ keV})^3 \sim 4 \gg 1$  and microturbulence effects dominate there [21]. While such an effect may help initiate an eITB in JT-60U, it is not relevant in the fully developed eITBs there. Rather, the strong reversed shear inside  $q_{\text{min}}$  decreases the collisionless  $\chi_{e1}^{\text{pc}} \sim |q'|^{-1/2}$  there—as shown in figures 11 and 12. The RTP-type eITBs around low order rational surfaces are not likely to be observable in

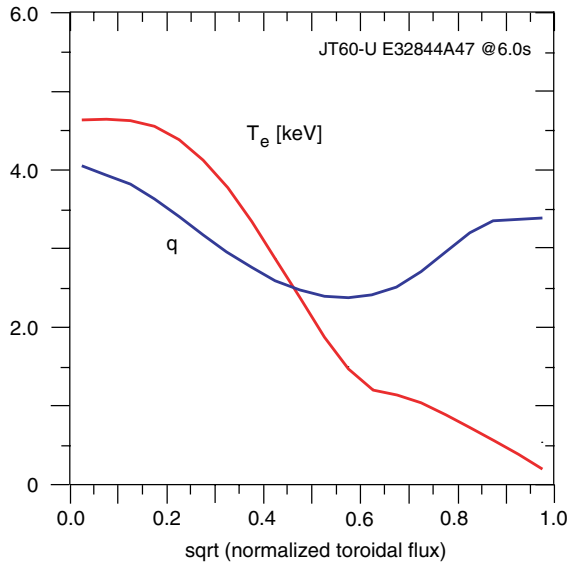


**Figure 11.** Profiles of  $T_e$ ,  $q$  in JT-60U for a strong eITB, which is inside  $q_{\min}$  at  $\rho \simeq 0.575$ .

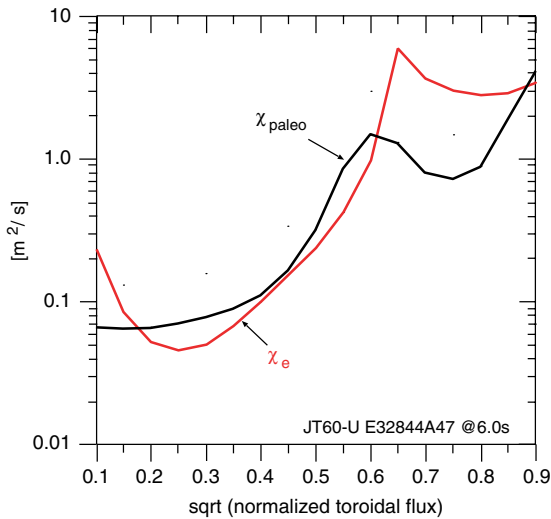


**Figure 12.** Comparison of TRANSP and paleoclassical  $\chi_e$  for the JT-60U case in figure 11.

this JT-60U discharge because the  $q$  profile is still evolving at 6.0s, which is short compared with the global magnetic diffusion time scale of  $\tau_\eta \sim 20$ s—see discussion of RTP temporal evolution at the end of the preceding paragraph. If the anomalous transport due to micro-turbulence is negligible,  $\chi_{\text{el}}^{\text{pc}}$  can produce the low, irreducible minimum level of electron heat transport. An example of this behaviour for a strong eITB in JT-60U, for which  $T_e^{\text{crit}} \simeq 2.4$  keV, is shown in figures 11 and 12. The TRANSP analysis (figure 12) shows that the eITB occurs primarily inside the  $q_{\min}$  surface at  $\rho \simeq 0.575$  and that the reduction in  $\chi_e$  there is well represented by the ‘collisionless’ (I) paleoclassical model in this JT-60U discharge in which a ‘reduction in the size of the turbulent structures is observed ... during the evolution of the internal transport barrier’ [24]. Strongly reversed magnetic shear can also be important in the core of NSTX plasmas—see section 7 and figure 17.

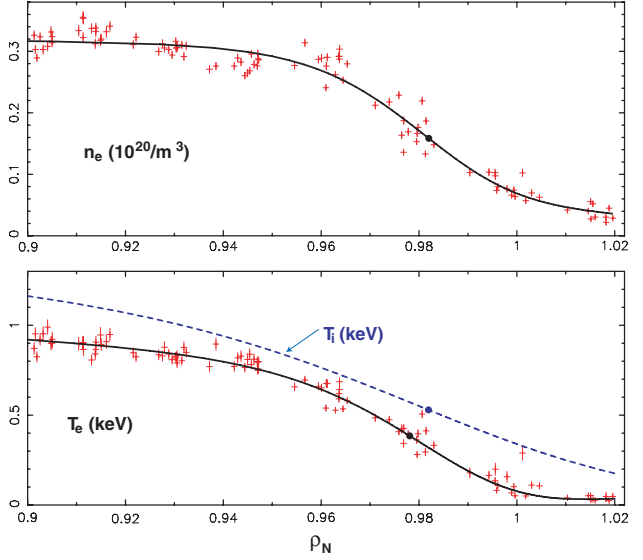


**Figure 13.** Edge pedestal  $n_e$  and  $T_e$  profiles for DIII-D shot 98889, averaged over 80–99% of time to next ELM crash, around 4500 ms.

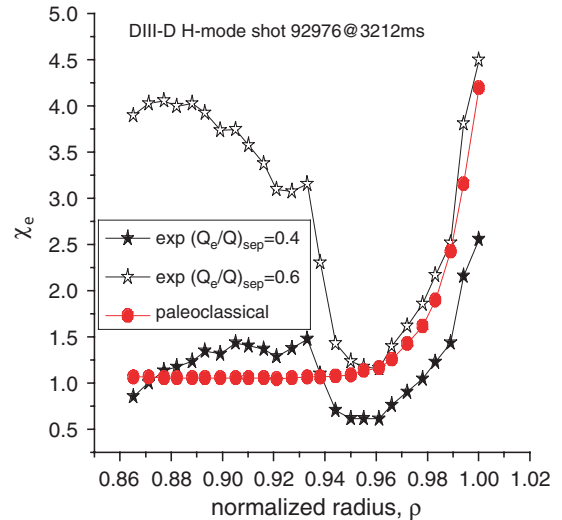


**Figure 14.** Transport analysis  $\chi_e$  ( $\text{m}^2 \text{s}^{-1}$ ) in DIII-D pedestal depends on electron fraction of power flowing through separatrix,  $(Q_e/Q)_{\text{sep}}$  [25].

## 6. H-mode edge $T_e$ pedestals in DIII-D

Figures 1, 2 and 5 show that as  $\rho$  approaches the separatrix,  $\chi_e^{\text{pc}}$  is first in the collisional (II) regime where  $\chi_{\text{eII}}^{\text{pc}} \propto T_e^{1/2}/n_e q$  decreases with increasing  $\rho$ . Further out where  $\lambda_e < \pi R q$  one has  $M < 1$ ; in this edge region (III)  $\chi_{\text{eIII}}^{\text{pc}} \propto T_e^{-3/2}$  increases as  $T_e$  decreases further. Edge pedestal  $n_e$  and  $T_e$  profiles are shown in figure 13 for a well-diagnosed DIII-D H-mode discharge with 36 ms between ELM crashes. Figure 14 shows a comparison of  $\chi_e^{\text{pc}}$  with results from an integrated transport analysis code [25] of a similar DIII-D shot 92976, which had a higher pedestal density  $n_e^{\text{ped}} \simeq 4.3 \times 10^{19} \text{ m}^{-3}$  but lower  $T_e^{\text{ped}} \simeq 300$  eV. The paleoclassical  $\chi_e$  compares reasonably favourably with the experimentally inferred  $\chi_e$  for most cases analysed to date [26, 27], especially in the near separatrix region ( $\rho > 0.96$ ) where  $\chi_{\text{eIII}}^{\text{pc}} \propto T_e^{-3/2}$ . The increase of  $\chi_{\text{eIII}}^{\text{pc}}$

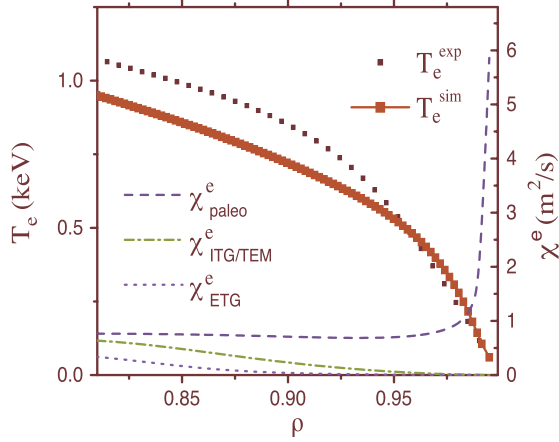


**Figure 15.** ASTRA modelling [28] of DIII-D edge  $T_e(\rho)$  like that in figure 13 with the paleoclassical model (using 500 radial points).

with  $\rho$  in the near separatrix region causes the  $T_e$  profile to have positive or neutral curvature there (i.e.  $\partial^2 T_e / \partial \rho^2 \geq 0$ ), for example outside the  $T_e$  ‘symmetry point’ at  $\rho = 0.978$  in figure 13. This aspect of the paleoclassical model is critical for producing appropriate ASTRA modelling [28] of the edge  $T_e$  pedestal, as illustrated in figure 15.

Paleoclassical predictions have been developed for the  $T_e$  profile in an H-mode edge pedestal region [29]. Near the separatrix  $M < 1$  and  $n_e T_e D_\eta \propto n_e / T_e^{1/2}$ ; thus, integrating equation (1) from the separatrix inwards the paleoclassical model predicts [29]  $T_e \propto n_e^2$  or  $\eta_e \equiv d \ln T_e / d \ln n_e \simeq 2$ , in agreement with ASDEX-U [30] and DIII-D data very close to the separatrix ( $T_e \lesssim 200$  eV) [29]. This relation applies up to the point ( $\rho \lesssim 0.985$  in figures 13 and 15 but  $\lesssim 0.94$  in figure 14), where  $\lambda_e \gtrsim \pi R q / 2$  and  $M \gtrsim 0.5$ , beyond which  $\chi_e^{\text{pc}}$  stops decreasing or reaches a minimum and causes a maximum  $|\nabla T_e|$ . Further inwards, the collisional regime  $\chi_{\text{el}}^{\text{pc}}$  is nearly constant, but  $\chi_e$  from ITG/TEM modes increases rapidly (for  $\rho < 0.9$  in figure 15). The  $T_e$  at the top of the pedestal is predicted by balancing collisional regime (II) paleoclassical transport against gyro-Bohm-scaled anomalous electron heat transport. This yields a prediction [29] of  $\beta_e^{\text{ped}} \equiv n_e^{\text{ped}} T_e^{\text{ped}} / (B^2 / 2\mu_0) \simeq (0.032 / f_\# A_i^{1/2}) (\bar{a} / R q) (\eta_{\parallel}^{\text{nc}} / \eta_0)$ , which is reasonably consistent with the DIII-D pedestal database for  $f_\# \sim 0.6$ – $2$ — see figure 16.

## 7. Non-tokamak experiments: ST/NSTX, RFP/MST, spheromak/SSPX

The paleoclassical model [1, 3] applies to axisymmetric resistive, current-carrying toroidal plasmas of all types—spherical tokamaks (STs), reversed field pinches (RFPs) and spheromaks—in regions where  $\epsilon^2$ ,  $B_p^2 / B_t^2 \ll 1$ . Figure 17 shows that the paleoclassical model captures the decrease in core  $\chi_e$  caused by moderately reversed shear ( $q' < 0$  for  $\rho < 0.45$ ) in an ohmic-level NSTX L-mode plasma, analogous to the  $\rho < 0.6$  JT-60U results in figure 12. The dashed line in figure 17 indicates the region where the zero shear,  $\max\{n_{\text{max}}\}$  formula in (6) has been used. Figure 18 shows the ratio of the TRANSP analysis  $\chi_e$  to the collisionless regime (I) paleoclassical  $\chi_{\text{el}}^{\text{pc}}$  at  $\rho = 0.65$  for a variety of L-mode NSTX

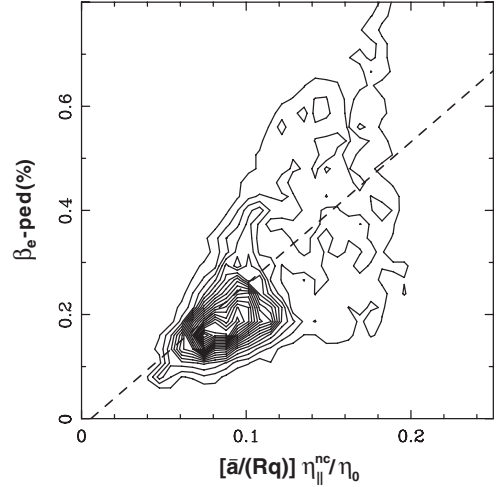


**Figure 16.** DIII-D database of  $\beta_e^{\text{ped}}$  (in %) versus the paleoclassical  $\beta_e^{\text{ped}}$  parameter  $(\bar{a} / R q) (\eta_{\parallel}^{\text{nc}} / \eta_0)$ . Slope of the fitted line corresponds to  $f_\# \simeq 0.8$ .

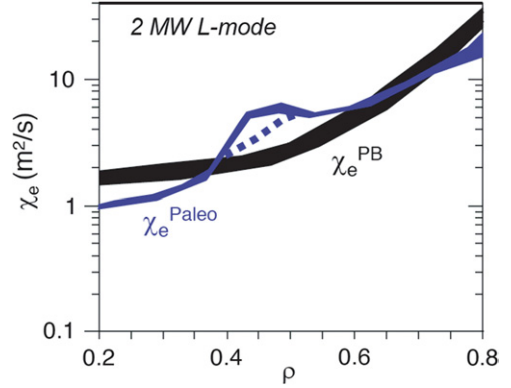


**Figure 17.** TRANSP and paleoclassical  $\chi_e$  for L-mode NSTX reversed shear plasma [31].

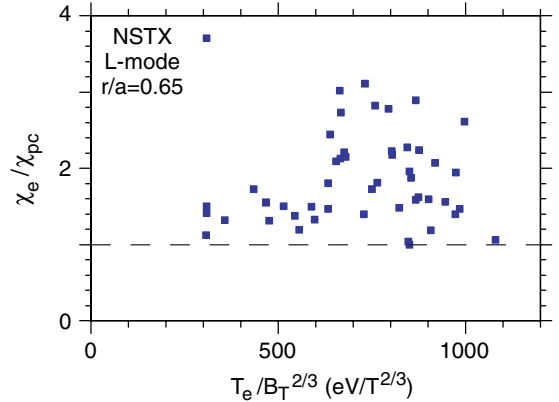


**Figure 18.** Ratio of TRANSP to paleoclassical  $\chi_e$  versus  $T_e^{\text{crit}}$  parameter for NSTX L-mode discharges.

discharges from the 2004 and 2005 campaigns. Two points about it are notable: (1) since all the data have ratios of about unity or greater, the paleoclassical  $\chi_{\text{el}}^{\text{pc}}$  is setting the irreducible minimum electron thermal diffusivity and (2)  $\chi_e$  is usually at the collisionless (I) paleoclassical level for  $T_e$  less than about  $0.65 B_T^{2/3}$  keV, but often above it for larger  $T_e$ . Similar

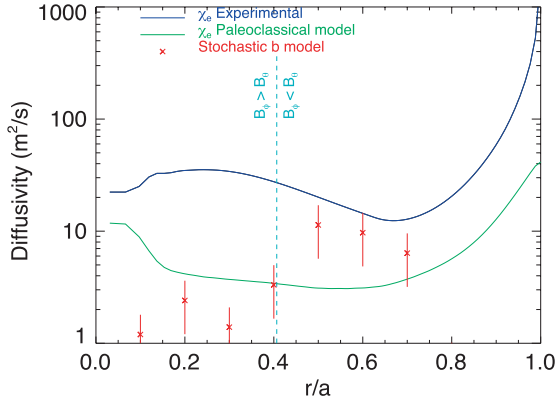


**Figure 19.**  $\chi_e$  in quiescent (PPCD) MST plasmas [32]; transport is not below the paleoclassical level.

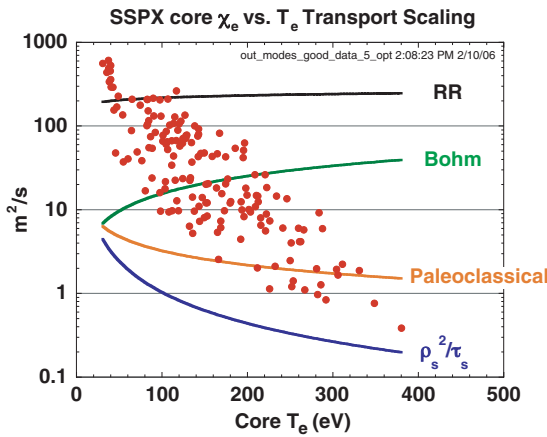


**Figure 20.** SSPX  $\chi_e$  on axis decreases as  $T_e$  increases [33]; paleoclassical may limit at high  $T_e$ .

comparisons for  $\rho = 0.4$  in L-mode discharges and higher heating power NSTX H-mode discharges find that: (1) the TRANSP  $\chi_e$  usually significantly exceeds  $\chi_e^{pc}$  throughout the plasma, (2) their minimum ratio is never below 0.5, has a mean of about 4 and ranges up to 13 and (3) all ratios have  $T_e/B^{2/3} \geq 0.5$  keV. Since for these NSTX discharges  $\kappa \simeq 1.9$  and  $\bar{a} \simeq 0.8$  m, this implies that for these discharges  $T_e^{crit} \simeq (0.55\text{--}0.72) B^{2/3}\bar{a}^{1/2}$  keV, which is less than a factor of two smaller than (11), or alternatively indicates  $f_{\#} \sim 1\text{--}2$ .

For quiescent RFP plasmas such as those in MST PPCD discharges [32], the magnetic fluctuations due to tearing modes are reduced; thus, the magnetic-flutter-induced transport is reduced and the electron heat transport is reduced to tokamak levels. Figure 19 shows that the  $\chi_e$  in these PPCD discharges is less than an order of magnitude above and has approximately the same profile as the collisionless regime (I) paleoclassical  $\chi_{el}^{pc}$ .

In the SSPX spheromak [33], as shown in figure 20, in  $T_e \sim 100$  eV plasmas  $n = 1$  magnetic fluctuations are present and produce a magnetic-flutter level  $\chi_e$  (RR—Rechester–Rosenbluth). As  $T_e$  is increased (via magnetic flux increases), both magnetic fluctuations and  $\chi_e$  decrease. As indicated in figure 20, for  $T_e \gtrsim 200$  eV the collisional regime paleoclassical  $\chi_{el}^{pc}$  may set the lower limit on electron heat transport.

## 8. Conclusions about paleoclassical electron heat transport

From these studies, we conclude that paleoclassical transport sets the irreducible minimum electron heat transport level in many resistive, current-carrying toroidal plasmas (factor  $\lesssim 2$  in tokamaks,  $< 10$  in RFPs and spheromaks)—for  $T_e \lesssim T_e^{crit} \equiv B^{2/3}\bar{a}^{1/2}(3f_{\#})^{-1/3}$  keV where it is expected to be dominant unless exceeded by fluctuation-induced transport due to RBMs for  $T_e \lesssim 300$  eV in L-mode plasmas, magnetic fluctuations (Rechester–Rosenbluth  $\chi_e$ ), or core ( $\rho \lesssim 0.4$ ) sawtooth effects. For  $T_e > T_e^{crit}$  ( $\sim 0.7\text{--}2.4$  keV in present devices but  $\sim 3.5\text{--}5$  keV in ITER) anomalous transport due to drift-type micro-turbulence (ITGs, TEMs, ETGs) with a gyro-Bohm diffusivity  $\chi_e^{gB} \equiv f_{\#}(Q_S/\bar{a})(T_e/eB)$  is more likely to be dominant, unless it is stabilized by  $E \times B$  flow shear. Comparisons here indicate  $1/3 \lesssim f_{\#} \lesssim 2$ ; fortunately this large uncertainty in  $f_{\#}$  results in less than a factor of two uncertainty in  $T_e^{crit}$ .

## Acknowledgments

This research was supported by US DoE grants and contracts DE-FG02-92ER54139 and DE-FC02-05ER54184 (UW-Madison), DE-FC02-04ER54698 (GA), DE-FG02-92ER54141 (Lehigh), DE-AC02-76CH03073 (PPPL), DE-FG02-99ER54512 (MIT), DE-AC05-00OR22725 (ORNL), W-7405-ENG-48 (LLNL), DE-FG02-00ER54538 (GaTech) and DE-FG02-99ER54523 (JHU). The JAEA work was supported by the Japan Society for the Promotion of Science. The FOM work was supported by the EC European Fusion Programme and NWO.

## References

- [1] Callen J.D. 2005 *Nucl. Fusion* **45** 1120
- [2] Callen J.D. 2005 *Phys. Rev. Lett.* **94** 055002
- [3] Callen J.D. 2005 *Phys. Plasmas* **12** 092512
- [4] Callen J.D. 2006 *Phys. Plasmas* **14** 040701
- [5] Camenen Y. *et al* 2005 *Plasma Phys. Control. Fusion* **47** 1971
- [6] Petty C.C., Luce T.C., DeBoo J.C., Waltz R.E., Baker D.R. and Wade M.R. 1998 *Nucl. Fusion* **38** 1183
- [7] Petty C.C. and Luce T.C. 1999 *Phys. Plasmas* **6** 909
- [8] Arlen T.C., Greenfield C.M., St John H.E. and Callen J.D. 2005 *Bull. Am. Phys. Soc.* **50** 151
- [9] Greenfield C.M. *et al* 2006 *US Transport Task Force Meeting Myrtle Beach, SC* <http://www.mfescience.org/TTF2006>
- [10] Carreras B.A. *et al* 1993 *Phys. Rev. Lett.* **50** 503
- [11] Rogers B.N., Drake J.F. and Zeiler A. 1998 *Phys. Rev. Lett.* **81** 4396
- [12] Rettig C.L. *et al* 2001 *Phys. Plasmas* **8** 2232
- [13] Rettig C.L., Staebler G.M., Rhodes T.L., Doyle E.J., Peebles W.A. and Burrell K.H. 2001 *Plasma Phys. Control. Fusion* **43** 1273
- [14] Wade M.R. *et al* 2005 *Nucl. Fusion* **45** 407
- [15] Lazarus E.A. *et al* 2006 *Plasma Phys. Control. Fusion* **48** L65
- [16] Lazarus E.A. *et al* 2006 *Phys. Plasmas* **14** 055701
- [17] Greenwald M. *et al* 1997 *Nucl. Fusion* **37** 793
- [18] Lopes Cardozo N.J. *et al* 1997 *Plasma Phys. Control. Fusion* **39** B303
- [19] Hogewij G.M.D., Lopes Cardozo N.J., de Baar M.R. and Schilham A.M.R. 1998 *Nucl. Fusion* **38** 1881
- [20] Hogewij G.M.D., Callen J.D. and de Blank H.J. 2006 Paleoclassical electron internal transport barriers in RTP

- Proc. 33rd Eur. Conf. on Controlled Fusion and Plasma Physics (Roma, Italy, 2006)* CD-ROM file P-4.148
- [21] Austin M.E. *et al* 2006 *Phys. Plasmas* **13** 082502
- [22] Fujita T. *et al* 1997 *Phys. Rev. Lett.* **78** 2377
- [23] Fujita T. *et al* 2004 *Plasma Phys. Control. Fusion* **46** A35
- [24] Nazikian R. *et al* 2005 *Phys. Rev. Lett.* **94** 135002
- [25] Stacey W.M. and Groebner R.J. 2006 *Phys. Plasmas* **13** 072510
- [26] Stacey W.M. and Evans T.E. 2006 *Phys. Plasmas* **13** 112506
- [27] Stacey W.M. and Groebner R.J. 2007 *Phys. Plasmas* **14** 012501
- [28] Pankin A.Y. *et al* 2006 *Nucl. Fusion* **46** 403
- [29] Callen J.D., Osborne T.H., Groebner R.J., St John H.E., Pankin A.Y., Bateman G., Kritz A.H. and Stacey W.M. 2007 Paleoclassical model for edge electron temperature pedestal, UW-CPTC 06-6 submitted
- [30] Horton L.D. *et al* 2005 *Nucl. Fusion* **45** 856
- [31] Stutman D. *et al* 2006 *Phys. Plasmas* **13** 192511
- [32] Sarff J.S. *et al* 2003 *Plasma Phys. Control. Fusion* **45** A457
- [33] McLean H.S. *et al* 2006 *Phys. Plasmas* **13** 056105